A Three-Dimensional Difference Map of the N Intermediate in the Bacteriorhodopsin Photocycle: Part of the F Helix Tilts in the M to N Transition[†]

Janet Vonck*,[‡]

Lawrence Berkeley National Laboratory, Life Sciences Division, Donner Laboratory, University of California, Berkeley, California 94720

Received November 8, 1995; Revised Manuscript Received February 1, 1996[⊗]

ABSTRACT: The N intermediate of the bacteriorhodopsin photocycle was trapped for electron diffraction studies in glucose-embedded specimens of the site-directed mutant Phe219→Leu. At neutral pH, the N-bR difference Fourier transform infrared spectrum of this mutant is indistinguishable from published difference spectra obtained for wild-type bacteriorhodopsin at alkaline pH. An electron diffraction difference map of the N intermediate in projection shows large differences near the F and the G helix, which are very similar to the features seen in the M intermediates of the Asp96→Gly mutant [Subramaniam et al. (1993) *EMBO J. 12*, 1−8]. This similarity was anticipated on the basis of Fourier transform infrared data, which have shown that the M intermediate trapped in Asp96 mutants already has the protein structure of the N intermediate [Sasaki et al. (1992) *J. Biol. Chem. 267*, 20782−20786]. A preliminary three-dimensional difference map of the N intermediate, calculated from electron diffraction data of samples tilted at 25°, clearly shows that the change on the F helix consists of an outward movement of the cytoplasmic end of the helix. In addition, the cytoplasmic side of the G helix moves or becomes more ordered. Comparison with published difference maps of the M intermediate indicates that the F helix tilt occurs in the M to N transition, but the G helix change represents an earlier step in the photocycle.

It is becoming increasingly clear that a significant structural change occurs during the light-driven proton pumping cycle of bacteriorhodopsin. This seven α-helix transmembrane protein occurs in crystalline patches in the purple membrane of *Halobacterium salinarium* and was the first membrane protein for which the structure was solved by electron crystallography (Henderson et al., 1990). The initial light-driven reaction is the isomerization of the retinal prosthetic group from an *all-trans* to a 13-*cis* configuration. Proton transfer starts when the Schiff base, connecting the retinal to Lys216 in the middle of the seventh α-helix, becomes deprotonated and Asp85, located on the extracellular side, becomes protonated (Braiman et al., 1988, 1991; Otto et al., 1990). After this a structural change is believed to take place which provides access to the Schiff base from the cytoplasmic side. The Schiff base is then reprotonated from Asp96 (Holz et al., 1989; Gerwert et al., 1989; Otto et al., 1989; Bousché et al., 1991), which is located halfway between the Schiff base and the cytoplasmic surface (Henderson et al., 1990).

Different stages in the photocycle have been identified traditionally on the basis of their visible light absorption, which is modified by the interaction of the retinal with the protein (Lozier et al., 1975). The initial photoreaction transforms the ground state bR_{570}[1] into K_{590}, which has a strained 13-*cis*-retinal. The retinal is relaxed in L_{550}; the Schiff base deprotonates in the transition to M_{412} and reprotonates in $M \rightarrow N_{550}$. In O_{640} the retinal is back in the *all-trans* configuration, and all remaining changes are reversed in O→bR. [For reviews see Mathies et al. (1991), Lanyi (1993), and Krebs and Khorana (1993).]

However, it is now clear that structural changes occur in the photocycle that do not influence the visible spectrum but can be resolved by other methods, such as Fourier transform infrared spectroscopy (FTIR). In particular, it is known that the protein structure of the M intermediate, which owes its very distinct color to the deprotonated Schiff base, can exist in at least two and perhaps three different conformations. A clear indication of this was given in the work by Váró and Lanyi (1991a−c), showing kinetic evidence for two M substates, which they named M_1 and M_2, linked by an irreversible step. The nature of this transition is still unclear, however. Secondly, Sasaki et al. (1992) showed by FTIR that the long-lived M state in Asp96 mutants, which they called M_N, actually has the protein structure of the wild-type N intermediate although the Schiff base is still deprotonated due to slowed proton transfer from the bulk phase. This finding shows that a protein structural change precedes the reprotonation of the Schiff base from the cytoplasmic side.

Several lines of evidence suggest that the protein structural changes that occur during the M state are the biggest ones in the photocycle and probably include a tilt of the cytoplasmic side of the F helix. FTIR difference spectra of N-bR show peaks in the amide I region that are larger than at any other stage in the photocycle (Pfefferlé et al., 1991; Braiman et al., 1991; Ormos et al., 1992). An electron diffraction difference map of the M state of the D96G mutant shows difference peaks compatible with a tilt of the cytoplasmic part of the F helix (Subramaniam et al., 1993). Site-directed isotope labeling and ATR-FTIR difference spectroscopy indicate that the backbone of Tyr185, which

[†] This work was supported by NIH Grant GM51487.

[‡] Present address: European Molecular Biology Laboratory, Meyerhofstrasse 1, Postfach 10.2209, D-69012 Heidelberg, Germany.

[⊗] Abstract published in *Advance ACS Abstracts,* April 15, 1996.

[1] Abbreviations: bR, bacteriorhodopsin; FTIR, Fourier transform infrared spectroscopy; 2-D, two dimensional; 3-D, three dimensional.

S0006-2960(95)02663-8 CCC: $12.00

is connected to Pro186 in the F helix, is structurally active during the M to N transition (Ludlam et al., 1995). Introducing bulky groups near the cytoplasmic surface on helix F, but not others, has a large influence on the kinetics of M and N decay (Brown et al., 1995).

To determine the nature of this structural change in more detail, three-dimensional information is needed, which can be obtained from electron diffraction data of tilted samples. The present study shows a limited-resolution 3-D difference map of the N intermediate. Because the N state of wild-type bR can only be trapped at high pH, and even then occurs in a mixture with other intermediates, in the present work the N intermediate was trapped in the F219L mutant (Brown et al., 1994), which has a long-lived N intermediate at neutral pH. The N-bR electron diffraction difference map obtained in projection looks very similar to the M (actually M_N) map from the D96G mutant (Subramaniam et al., 1993), with large difference peaks near the F and G helix. This close similarity is consistent with the fact that the FTIR changes of the intermediates that were trapped in the F219L mutant and in the D96N mutant (closely related to the D96G mutant) are also very similar. A 3-D difference map from 25° tilted samples confirms that the change on the F helix represents a tilt of the cytoplasmic half of helix F out into the lipid region, away from the center of the molecule. A change on the G helix is present in all M difference maps shown so far (Dencher et al., 1989; Koch et al., 1991; Nakasako et al., 1991; Subramaniam et al., 1993; Han et al., 1994a), as well as the present N map. It can therefore be concluded that the change on helix G occurs at an earlier step in the photocycle than the M to N transition.

MATERIALS AND METHODS

A *H. salinarium* strain containing the mutant bacteriorhodopsin F219L (Brown et al., 1994) was a gift from Dr. J. K. Lanyi. The purple membrane was isolated by standard methods (Oesterhelt & Stoeckenius, 1974).

Glucose-embedded, hydrated FTIR samples were prepared as described by Perkins et al. (1992). FTIR spectra were taken essentially as described before (Vonck et al., 1994), at several temperatures between 260 and 280 K, at 2 cm^{-1} resolution. In order to obtain FTIR difference spectra of N-bR, first a set (typically 300) of bR scans were taken in the dark. Then the sample was illuminated with green light, and 10 intermediate scans, at a rate of about 1 s per scan, were collected immediately after turning off the light. Because of the relatively fast decay of the N intermediate at these temperatures, a cycle of illumination and scanning could be repeated several times without heating the sample. Typically, data were collected from 30 cycles per experiment. All the N scans were averaged, and the bR average was subtracted to obtain a difference spectrum.

For electron diffraction, the purple membranes were fused to larger sizes (Baldwin & Henderson, 1984). Glucose-embedded, hydrated samples were prepared as described (Han et al., 1994a), using molybdenum grids (Booy & Pawley, 1993) and Fullam 120−30 carbon (Ernest Fullam Inc., Latham, NY). This combination gives a high proportion of flat crystals at low temperatures (Han et al., 1994b), which is essential for recording electron diffraction data from tilted specimens.

Trapping of the N intermediate on electron microscope grids was done essentially by the procedure described by Han et al. (1994a) for the M intermediate, except for the higher temperature. Briefly, the grid was plunged into liquid nitrogen, in the dark, then heated to 270 K and illuminated for 30 s with green light to form N, or kept in the dark for bR, and rapidly cooled with liquid nitrogen to prevent N decay.

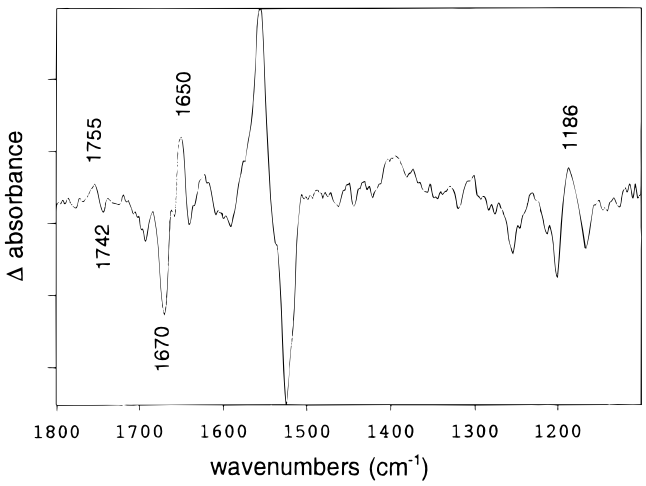

FIGURE 1: Fourier transform infrared N-bR difference spectrum of glucose-embedded Phe219→Leu bacteriorhodopsin at −3 °C. Difference peaks that are discussed in the text are indicated.

The grid was observed in a JEOL JEM 4000EX electron microscope at temperatures below −120 °C, using an accelerating voltage of 400 kV, with the sample either untilted or at 25° tilt. Electron diffraction data were collected on Kodak SO-163 film or on a Gatan slow-scan CCD camera. When the CCD camera was used, several successive images (typically eight) obtained with short exposures were collected at a total electron dose of approximately 2 $e^-/Å^2$ and added up. This procedure reduced the "bloom steak", caused by the oversaturated area of the unscattered beam (Brink & Chiu, 1994).

The data were processed using the MRC set of programs developed by Baldwin and Henderson (1984). The diffraction intensities were extracted from the data as described by Ceska and Henderson (1990). The intensities from the bR and the N state were first merged to the reference curves of Ceska and Henderson, after which new curves were obtained by iterative cycles of curve fitting and remerging. Fourier difference maps were calculated from the difference amplitudes and the experimental phases that were used to construct the atomic model (Henderson et al., 1990).

RESULTS

Purple membranes embedded in amorphous ice have been, in general, insufficiently flat for the collection of data from tilted samples, necessary for 3-D reconstructions. Glucose embedding, on the other hand, can alter the hydration level, which has a profound effect on the photocycle of bR (Perkins et al., 1993). FTIR spectroscopy was therefore used to establish suitable conditions to trap the N intermediate in glucose-embedded samples, which were partially hydrated in an atmosphere of 80% relative humidity (Perkins et al., 1993). Illumination of such a sample at neutral pH (as well as at pH 10) and a temperature of 270 K gave an FTIR spectrum for the glucose-embedded F219L mutant (Figure 1) that was very similar to published N spectra (Pfefferlé et al., 1991; Braiman et al., 1991; Ormos et al., 1992). In

particular, the 1650/1670 cm^{-1} positive/negative peak pair, the positive peak at 1186 cm^{-1}, and the 1755 cm^{-1} peak, which all occur in N but not in M, are clearly present. The relative heights of the most important peaks (1650/1670 cm^{-1} and 1186 cm^{-1} versus 1526/1557 cm^{-1}) were the same as those in the N spectrum of Ormos et al. (1992), which was calculated by subtracting the M contribution from an M/N mixture produced at 260 K. It can be concluded that any remaining M in the spectrum in Figure 1 will be very low. At lower temperatures (260 or 265 K), more noticeable amounts of M were present, as evidenced by a lowered peak at 1186 cm^{-1}, a smaller 1650 and 1670 cm^{-1} peak, and a larger 1659 cm^{-1} peak. Higher temperatures were less favorable because the decay time of the N state became faster. At 270 K, the half-life of N was estimated as 8 s, which is sufficiently long to trap most molecules in the N state in the electron microscope samples, where the grid can be cooled within 1 or 2 s after illumination. Thus in order to get the highest possible proportion of the N intermediate and a suitably long lifetime, a temperature of 270 K was used for collection of electron diffraction data.

Electron diffraction patterns were collected from glucose-embedded samples prepared under the same conditions of humidity and temperature as the FTIR samples, with the samples either untilted or at 25° tilt. The patterns were indexed and their tilt axis and tilt angles calculated using the MRC programs. The diffraction intensities were fitted to the bR reciprocal lattice curves from Henderson et al. (1990). The Friedel *R*-factor, R_{sym}, was calculated for each film. R_{sym} is a measure for the quality of each film and is defined as

$$R_{sym} = \sum|I_1 - I_2|/\sum I_{curve}$$

where I_1 and I_2 are the diffraction intensities of two Friedel mates (Baldwin & Henderson, 1984). R_{sym} was between 5% and 10% for all diffraction patterns, both of the bR and of the N state. The diffraction data were merged to the bR curves from Henderson et al. (1990), and the merging *R*-factor was calculated:

$$R_{merge} = \sum|I_{obsd} - I_{curve}|/\sum I_{curve}$$

When only the diffraction patterns from untilted samples were considered, the initial value for R_{merge} for bR was 18.1 ± 1.3% and that for the N intermediate was 24.7 ± 2.6%. This significant difference in R_{merge} values between the bR state and the N intermediate indicates that there are measurable light-induced changes between the two states. The difference in the R_{merge} values between the bR and N data sets was less when the tilted data were used: for bR the average R_{merge} was 22.5 ± 3.0% and for the N-intermediate films 25.4 ± 2.1%. After new lattice line curves were fitted to the data points and the diffraction patterns were merged against these new curves, the average R_{merge} was 10.3 ± 1.2% for the bR data and 9.1 ± 1.4% for the N data, showing excellent internal consistency in both data sets. Further cycles of refinement showed minimal changes.

An N-bR Fourier difference map was calculated in projection at 3.5 Å resolution from 12 N and 16 bR patterns, all from untilted samples, using the phase information from Henderson et al. (1990). The main features in this projection map, shown in Figure 2, are two large positive peaks and a negative peak between them, in the region of helices F and G. Several minor peaks are also present, some of which are similar in position to peaks in previously published intermediate projection maps.

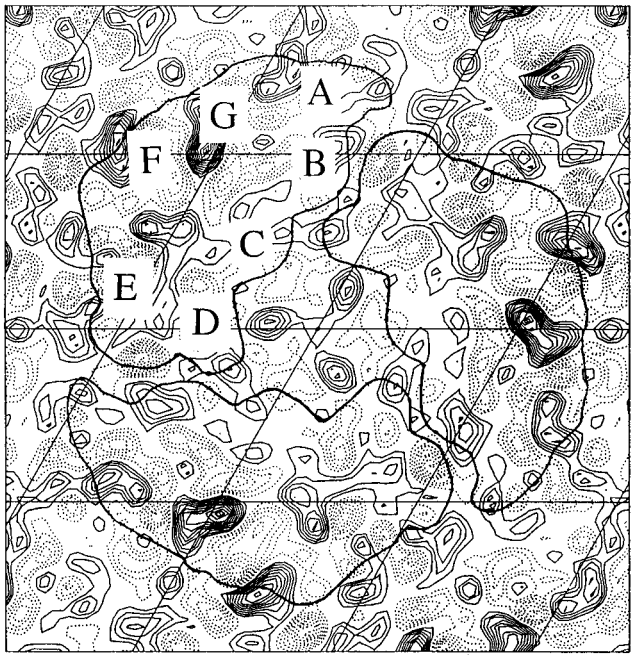

FIGURE 2: Difference Fourier map of N-bR in projection. The outline of three monomers is indicated, as well as the approximate position of the helices in one monomer. The distance between grid lines is 20.8 Å or one-third of a unit cell.

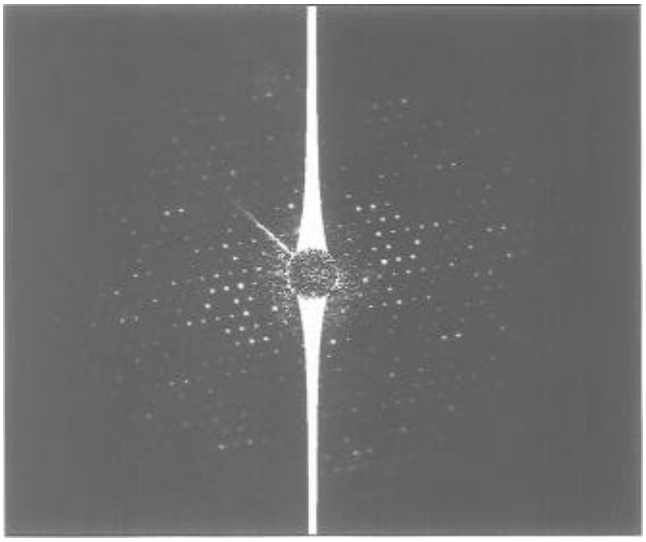

FIGURE 3: Electron diffraction pattern of Phe219→Leu bacteriorhodopsin in the N state at 25° tilt. The pattern was recorded on a slow-scan CCD; the radial background has been subtracted.

A 3-D difference map was calculated from the diffraction data of the untilted samples and 25° tilted samples (a total of 45 bR patterns and 37 N patterns), using only diffraction patterns with isotropically sharp spots (indicating flat crystals), like the example shown in Figure 3. The 3-D difference map is represented as a series of 2-D sections in Figure 4. In this map the approximate vertical position of the difference peaks that were seen in the projection map becomes clear. The positive and negative pair of peaks that occurs near the F helix in the projection map is located near the cytoplasmic surface of the protein. The positive peak on the G helix is also mainly located near the cytoplasmic side, but in addition

some positive density on the G helix extends further down. There is no large negative density associated with the G helix, but many smaller negative peaks surround the positive peak. Most of the remaining, small differences also occur in the outer, lipid-facing helices of the trimer (E, F, G, and A) with very little change showing up on helix B, C, or D at any vertical level. A more detailed description of the difference peaks will be given below.

DISCUSSION

Quality of the Difference Maps. 3-D reconstructions made using data from tilted samples have a reduced resolution in the vertical direction, caused by the missing cone in reciprocal space (Hoppe & Hegerl, 1980; Glaeser et al., 1989). In the case of a 25° tilt angle, as was used here, the vertical resolution is worse than the in-plane resolution of 3.5 Å by a factor of 3.0 (K. H. Downing, unpublished results), or about 10.5 Å (when apart from the missing cone reciprocal space is sufficiently well sampled, as it was in the present work). However, in the 3-D map of only 10° tilted samples of the M intermediate of the D96G mutant by Subramaniam et al. (1993), it was already evident that the most important changes were restricted to the cytoplasmic side of the protein. This is clearly confirmed by the present study. Although the vertical resolution is still too poor to interpret the difference peaks in atomic detail, several features that were visible in the projection maps can now be assigned a vertical position, as will be described below.

Differences between bR and the M and N Intermediates. The position and even the shape of the large peaks in the projection difference map of the N intermediate from F219L are remarkably similar to the M intermediate of the D96G mutant (Subramaniam et al., 1993). Similarities in the two structures were expected from the FTIR spectra: Sasaki et al. (1992) demonstrated the existence of an intermediate in the D96N mutant which retained a deprotonated Schiff base, specific for M, but had the protein structure of N, as indicated by the large 1670/1650 cm^{-1} peak pair in the amide I region. This M (yellow) intermediate, which is referred to as M_N, seems to be stabilized whenever there is no proton available to reprotonate the Schiff base, after the protein structure has changed from the "M" structure to the "N" structure. Wild-type bR which is insufficiently hydrated can also be trapped in the M_N state (Vonck et al., 1994). The M_N intermediate does not accumulate in fully hydrated wild-type bR, however, apparently because the Schiff base is reprotonated immediately after the protein conformational change if the proton donor Asp96 is present as well as sufficient water to hydrate the β-carboxyl group of Asp96.

Several earlier diffraction studies have presented difference maps of the M intermediate, using electron, X-ray, or neutron diffraction (summarized in Table 1). All show peaks near the F and/or the G helix. Most of these studies were done before the M_N intermediate had been discovered. As a result, the relative amounts of the M and M_N states present in the earlier experiments were not characterized. The distinction between M and M_N is a very important one, as the transition between them involves probably the largest conformational change in the photocycle. With the present knowledge these maps can be reinterpreted to determine which M substate was trapped.

There is little doubt that maps of the M intermediate which were obtained with bR from an Asp96 mutant (Koch et al., 1991; Subramaniam et al., 1993) can be interpreted as showing M_N, which has the N protein structure (Sasaki et al., 1992). Like the present N map, they both show peaks on helix F as well as helix G. Nakasako et al. (1991) added arginine at high pH, which was shown to prolong the lifetime of M (Nakasako et al., 1989). It can be shown by FTIR that this procedure actually traps M_N (J. Vonck, unpublished results). Both the F and G helix peaks are again present in the map. In the neutron diffraction map from Dencher et al. (1989), M was trapped by adding guanidine hydrochloride. This probably acts by the same mechanism as arginine (Nakasako et al., 1989) and by this argument should also trap mainly M_N. As would be predicted, the F helix peak pair and the G helix are both present.

The study by Han et al. (1994a) is the only one where the protein substate−composition of the M state was directly determined by FTIR. Wild-type bR samples embedded in glucose were illuminated at 240 and 260 K, where respectively pure M and an M/M_N mixture were produced (Vonck et al., 1994). Although the occupancy of the M state in samples prepared on electron microscope grids appears to have been rather low, judged by the relative peak heights in the available electron diffraction maps (Han et al., 1994a; Subramaniam et al., 1993; this study), it is clear that at 240 K the highest peak occurs on the G helix and at 260 K additional differences occur near the F helix. This suggests that the G helix change has already occurred in M and the F helix movement takes place during the M to M_N (or N) transition.

It can be deduced, therefore, that the protein structural change taking place just before the M→N transition (the Schiff base reprotonation) is a movement of the F helix. The changes that are seen on the G helix, however, are not coincident with this but occur at an earlier stage in the photocycle and have already occurred in M.

Comparison with the other difference maps presented by Subramaniam et al. (1993) confirms this picture. In wild-type bR, Subramaniam et al. trapped M by illuminating the sample at 5 °C and plunging the grids into liquid nitrogen within 10 or 20 ms after illumination. For kinetic reasons, this was expected to trap mainly M with a low amount of N. These maps show the same G helix peak but no big changes on helix F. (The small negative peak in the F helix region probably belongs to the extracellular side of helix G; see below.)

Changes on the G Helix. The positive peak on helix G is not accompanied by a single, localized feature of negative density but instead by a series of small negative peaks which do not all coincide with the position of the atomic model in the 3-D map. The maps presented here therefore support the conclusion by Subramaniam et al. (1993) that the cytoplasmic end of the G helix becomes more ordered in the photocycle. Edholm et al. (1995) recently found in a molecular dynamics simulation that the helices of bR show rather large fluctuations on the cytoplasmic side, while the extracellular side is much more fixed. So it is possible that a structural change early in the photocycle reduces the flexibility of the G helix. However, the distribution and size of the negative peaks also suggest the alternative explanation that the G helix change is a unique movement, but the position of some side chains in the model is incorrect. Future work is needed to distinguish between these possibilities.

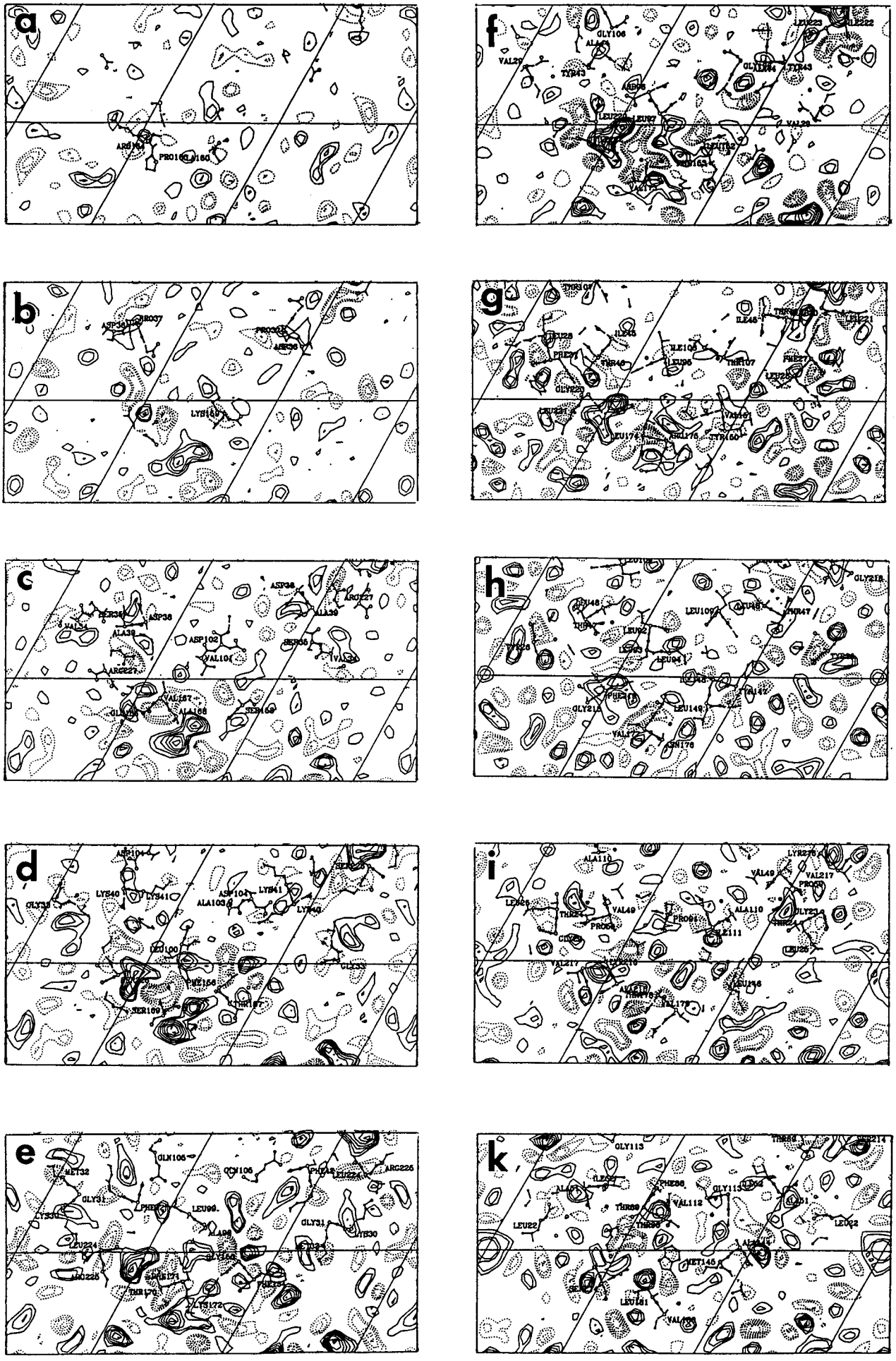
a
b
c
d
e
f
g
h
i
k

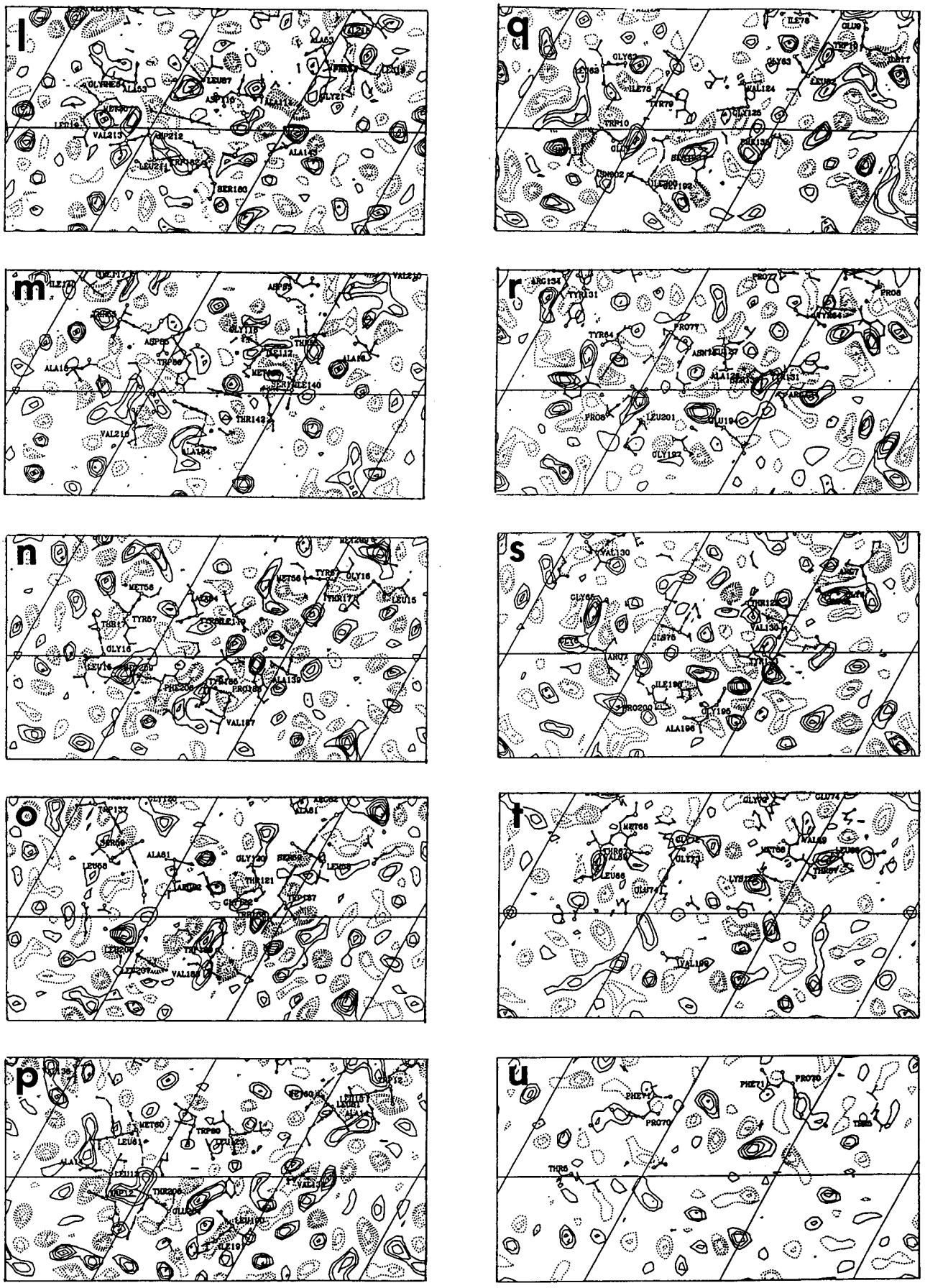

FIGURE 4: Sections of the N-bR 3-D difference Fourier map, spaced 2.8 Å apart, starting from the cytoplasmic side. The first section is 25 Å above the Schiff base (which is present in section k). Grid lines are at the same position as in Figure 2, 21 Å apart. The 3-fold axis in the center of the trimer is located at the intersection of the top of each panel with the middle grid line. On each section, the appropriate slice of the atomic model (Henderson et al., 1990) is indicated.

Table 1: Main Peaks Found in Published Diffraction Difference Maps of Bacteriorhodopsin Intermediates

authors	technique	trapping method	peaks near helices	interpretation
this study	electron diffraction	F219L mutant	F, G	N
Han et al., 1994	electron diffraction	wt, 260 K	F, G	M + M_N
Han et al., 1994	electron diffraction	wt, 240 K	G	M
Subramaniam et al., 1993	electron diffraction	D96G mutant	F, G	M_N
Subramaniam et al., 1993	electron diffraction	wt, 277 K, 20 ms	G	M
Nakasako et al., 1991	X-ray diffraction	wt, arginine, pH 9	F, G	M_N
Koch et al., 1991	X-ray diffraction	D96N mutant	B, F, G	M_N
Dencher et al., 1989	neutron diffraction	wt, guanidine hydrochloride	F, G	M_N

The point in the photocycle where the change on the G helix first occurs is not yet clear, as there are no published difference maps for intermediates earlier than M. The fact that this large change occurs on the helix that is connected to the retinal suggests that it is a direct consequence of the retinal isomerization or the Schiff base deprotonation and that the movement originates near Lys216, the residue to which the retinal is bound. In the 3-D model (Henderson et al., 1990), several of the α-helices are bent. Most kinks occur near proline residues, but helix G seems to be bent at the position of Lys216. This suggests that the conformation of helix G is influenced by the presence of the retinal, and it is not unreasonable to assume that the light-induced change occurring on the retinal (the isomerization and associated altered interaction with the binding pocket) could again induce a change on helix G. There is also direct evidence that the backbone of Lys216 undergoes conformational changes in the photocycle (Gat et al., 1992; Takei et al., 1994). Changes connected with the G helix residue Asp212, which plays an important although not yet quite understood role in the photocycle (Rothschild et al., 1990a; Needleman et al., 1991; Rath et al., 1993), may also be involved in altering the conformation of the G helix.

Although it is clear from the published projection maps (Table 1) that the G helix movement has already occurred in the M intermediate, it is not yet known when this change first takes place. It will be important to produce a difference map of the L intermediate to resolve this issue.

The F Helix Tilts in the M to N Transition. The 3-D difference map shows that the most prominent change in the M to N transition occurs on the cytoplasmic side of the F helix. Recently, indications that the cytoplasmic side of the F or the E helix, or the loop connecting them, can undergo conformational changes have come from several different sources. Steinhoff et al. (1994) showed with spin-labeled bR that either the C−D or the E−F loop changes during the M to N transition, but not earlier in the cycle. A molecular dynamics study by Edholm et al. (1995) found not only that the whole cytoplasmic side of the protein is flexible but also that the fluctuations are larger for the E−F loop and the connected helices than for the other components of the cytoplasmic domain. Müller et al. (1995) found by atomic force microscopy that altering the force on the cytoplasmic side of the protein caused a reproducible conformational change in the region of the E−F loop. It is intriguing that in G-protein-coupled receptors, another class of seven α-helix transmembrane proteins that includes rhodopsin, the loop connecting helices 5 and 6 (corresponding to E and F in bacteriorhodopsin) has been implicated in receptor/G-protein interactions, where conformational changes are also involved [reviewed in Strader et al. (1994)].

Subramaniam et al. (1993) suggested that the F helix movement in the photocycle is a tilt of the helix away from the main body of the protein, opening a channel from the cytoplasmic surface to the Schiff base. This suggestion is confirmed by the present 3-D map. The largest stretch of negative density in the map is located at the cytoplasmic end, between the two positive peaks, and coincides with the atomic model (Henderson et al., 1990) for the top of the F helix approximately from residue 167 to 177 (Figure 4c−h). The accompanying positive peak is located to the outside of the monomer, away from helix G. In the native state, the F helix is tilted relative to the membrane normal in the direction of helix G at the cytoplasmic side (Henderson et al., 1990), and the observed direction of tilt upon formation of the N intermediate implies that the cytoplasmic end of the F helix moves to a more vertical position. The FTIR spectrum of N shows larger protein changes than any other intermediate, with a negative peak at 1670 cm^{-1} and a positive peak at 1650 cm^{-1} (Braiman et al., 1991; Pfefferlé et al., 1991; Ormos et al., 1992). Rothschild et al. (1993) showed that this peak pair was due to an α-helical structure that is insensitive to hydrogen/deuterium exchange. Furthermore, they showed that the amide I band of bacteriorhodopsin consists of two subcomponents, one near 1670 cm^{-1} showing out of membrane plane dichroism and one near 1655 cm^{-1} exhibiting in-plane dichroism. As a result, they interpreted the positive/negative peak pair as a tilt of one or more α-helices toward the membrane normal, which changes the relative contributions of the in-plane and out-of-plane components of the amide I band. This interpretation of the FTIR data is in complete agreement with the observations described here.

It has been suggested that an F helix movement originates at the Tyr185−Pro186 bond. Several studies have shown that Pro186 plays an important role in the photocycle (Rothschild et al., 1990b; Ahl et al., 1989), and recently it was reported that the backbone of Tyr185 undergoes a change in the M to N reaction (Ludlam et al., 1995). A movement originating at Tyr185 and Pro186, which are part of the retinal binding pocket and close to key residues such as Asp85 and Asp212, seems very plausible. Tyr185 makes a polarizable hydrogen bond with Asp212 (Rothschild et al., 1990a; Olejnik et al., 1992), and this hydrogen bond undergoes significant changes during the photocycle (Rothschild et al., 1990a). Both of these residues are conserved in all halobacterial rhodopsins (Soppa et al., 1993).

Comparison of different bR mutants which form N-like protein structures shows that it is likely that the F helix movement is a consequence of the change in retinal geometry caused by the isomerization, rather than the Schiff base deprotonation. The D212N mutant, which does not have an M intermediate, displays the same light-induced diffraction intensity changes as the D96N mutant (Cao et al., 1993), which are again the same changes as in the F219L mutant, which have been identified here as arising from the N

intermediate protein structure. This shows that Schiff base deprotonation is not required for the F helix tilt to take place. Another mutant which can form an N-like protein structure without prior M formation is Y185F. Under light-adapted conditions, this protein exists partly as an O-like state, where Asp85 and Asp212 are protonated and the retinal is in the *all-trans* conformation. When this state is illuminated, the normal *all-trans* to 13-*cis* isomerization occurs and an N-like state is formed, as judged by the amide I bands (Sonar et al., 1993; Rath et al., 1993; He et al., 1993). So in this case as well, retinal isomerization apparently triggers the F helix movement. The same occurs in the mutant Y57D, where the Schiff base does not deprotonate, but an intermediate is formed which has an L-like chromophore but the N protein structure (Sonar et al., 1994). The D85N mutant has been shown to pump protons at pH 9, when the Schiff base is deprotonated, and the resulting photocycle includes an intermediate with the 1650/1670 cm^{-1} amide I peak pair (Nilsson et al., 1995). An earlier study by Kataoka et al. (1994) has however shown that D85N, at a pH above 11, without illumination already has the diffraction intensity changes associated with the M to N transition, and they concluded that the Schiff base deprotonation induces these changes. In view of the results by Nilsson et al. (1995), it appears now that another group than the Schiff base, with a pK_a around 11 in D85N, had become deprotonated in the Kataoka et al. experiment and had caused these normally light-induced changes. The fact that this does not occur in the wild-type protein (Kataoka et al., 1994) indicates that the pK_a of this unidentified group is lowered by the D85N mutation. The isomerization state of the retinal could not be determined under these conditions (Kataoka et al., 1994). It would be important for our understanding to see if this form of the protein has a 13-*cis* conformation as well.

The tilt of the F helix away from the main body of the protein produces an opening between the helices on the cytoplasmic side, which are tightly packed in the bR state (Henderson et al., 1990). This opening is probably large enough to allow water to have access to Asp96. Creation of such a channel supports a model proposed earlier to explain the proton transfer from Asp96 to the Schiff base (Vonck et al., 1994): Asp96 has an unusually high pK_a in the bR state, caused by its hydrophobic environment, but the β-carboxyl group can easily deprotonate when it is brought into contact with water through the newly opened channel. The released proton can then reprotonate the Schiff base. As predicted by this model, however, prior deprotonation of the Schiff base is not necessary for D96 deprotonation (Cao et al., 1993). It was shown by Cao et al. (1991) that relatively large amounts of water are needed for the Asp96 to Schiff base proton transfer. Also, FTIR data show that glucose-embedded, partially hydrated samples trap the M_N intermediate, where the channel has opened but the proton still resides on Asp96 (Vonck et al., 1994), under conditions where fully hydrated samples trap N (Ormos et al., 1992).

Other Difference Peaks. In the 3-D map, there are no big changes visible on the extracellular side of the protein (Figure 4m−u), of the same magnitude as those seen on the cytoplasmic side, where significant segments of helices are involved. Changes in the extracellular half of the protein are therefore likely to be restricted to single amino acids or otherwise be very limited in size. The poor vertical resolution of the present 3-D map does not yet allow an assignment of any peaks in this region. However, there are some features which deserve mention. A relatively large negative peak is visible on helix G around residue 207 or 208 (Figure 4n−o). This peak happens to coincide in projection with the much larger negative difference density on the F helix, much higher up in the structure. Because of the tilt of the helices relative to the membrane, the top of helix F is positioned directly above the extracellular end of helix G (Henderson et al., 1990). These two negative peaks contribute to the same peak in projection, and it is interesting to note that the extracellular, G helix peak is large enough to be visible by itself in projection maps: the difference maps lacking the positive F helix peak [the M_{240K} map of Han et al. (1994a) and the wild-type M map of Subramaniam et al. (1993)] still show a small negative peak on the position between the positive peaks, which in this case has to be the contribution from the G helix. The presence of the peak in these M intermediate maps suggests that a movement of the extracellular side of the G helix has already occurred in the M state, coincident with the change of the cytoplasmic part of helix G. In the 3-D map there is also a positive peak associated with the change on the extracellular end of helix G, which contributes to the large F helix peak in projection. A higher resolution of 3-D map should more accurately indicate the position where the smaller movements on the extracellular side occur.

Apart from the F and G helix peaks, some other differences are visible in many or all of the projection maps. The most important one is a positive/negative pair at the interface between the D or E helix of one monomer and the B helix of its neighbor in the trimer. In some maps (Dencher et al., 1989; Nakasako et al., 1991) this peak is as large as the G helix peak. Although this peak pair is visible in the N projection map as well, its vertical position is still ambiguous, as there is not a corresponding, single contribution that is evident in the present 3-D map. Another minor peak, visible only in the electron diffraction maps (which are of higher resolution than the X-ray and neutron diffraction maps), is a negative peak in the center of the monomer, close to the F helix peak. This peak corresponds to a large negative peak in the 3-D map which is located directly over the Schiff base (Figure 4k, l).

In ground state bR, the Schiff base is connected to the proton acceptor domain on the extracellular side, consisting of Asp85, Asp212, and Arg82. To ensure vectorial proton transport, access from the Schiff base to this complex must close after the Schiff base is deprotonated, and access to the cytoplasmic side, including Asp96, must open. This latter step is now identified as an opening of a water channel, caused by the movement of helix F. The closing of the extracellular access seems to be of a different nature, however, not being based on a clear movement of any helix but probably involving small changes in the relative positions of the members of the complex counterion, including water molecules. A higher resolution 3-D map may give a clearer picture of these events in the extracellular domain as well as any small changes that occur elsewhere in the protein.

ACKNOWLEDGMENT

I thank Bob Glaeser for his support, invaluable advice, many useful discussions, and comments on the manuscript.

I thank Janos Lanyi for providing the mutant strain and Felicia Hendrickson for isolating the purple membrane and for critical reading of an earlier version of the manuscript. I am grateful to Bong-Gyoon Han for his help with the MRC programs, to Rick Burkard for help with the FTIR and specimen preparation equipment, to David DeRosier for the loan of the slow-scan CCD camera, and to Ken Downing for his help with computer programs and the processing of CCD images.

REFERENCES

Ahl, P. L., Stern, L. J., Mogi, T., Khorana, H. G., & Rothschild, K. J. (1989) *Biochemistry 28*, 10028−10034.
Baldwin, J., & Henderson, R. (1984) *Ultramicroscopy 14*, 319−336.
Booy, F. P., & Pawley, J. B. (1993) *Ultramicroscopy 48*, 273−280.
Bousché, O., Braiman, M., He, Y.-W., Marti, T., Khorana, H. G., & Rothschild, K. J. (1991) *J. Biol. Chem. 266*, 11063−11067.
Braiman, M. S., Mogi, T., Marti, T., Stern, L. J., Khorana, H. G., & Rothschild, K. J. (1988) *Biochemistry 27*, 8516−8520.
Braiman, M. S., Bousché, O., & Rothschild, K. J. (1991) *Proc. Natl. Acad. Sci. U.S.A. 88*, 2388−2392.
Brink, J., & Chiu, W. (1994) *J. Struct. Biol. 113*, 23−34.
Brown, L. S., Yamazaki, Y., Maeda, A., Sun, L., Needleman, R., & Lanyi, J. K. (1994) *J. Mol. Biol. 239*, 401−414.
Brown, L. S., Váró, G., Needleman, R., & Lanyi, J. K. (1995) *Biophys. J. 69*, 2103−2111.
Cao, Y., Váró, G., Chang, M., Ni, B., Needleman, R., & Lanyi, J. K. (1991) *Biochemistry 30*, 10972−10979.
Cao, Y., Váró, G., Klinger, A. K., Czajkowsky, D. M., Braiman, M. S., Needleman, R., & Lanyi, J. K. (1993) *Biochemistry 32*, 1981−1990.
Ceska, T. A., & Henderson, R. (1990) *J. Mol. Biol. 213*, 539−560.
Dencher, N., Dresselhaus, G., Zaccai, G., & Büldt, G. (1989) *Proc. Natl. Acad. Sci. U.S.A. 86*, 7876−7879.
Edholm, O., Berger, O., & Jähnig, F. (1995) *J. Mol. Biol. 250*, 94−111.
Gat, Y., Grossjean, M., Pinevsky, I., Takei, H., Rothman, Z., Sigrist, H., Lewis, A., & Sheves, M. (1992) *Proc. Natl. Acad. Sci. U.S.A. 89*, 2434−2438.
Gerwert, K., Hess, B., Soppa, J., & Oesterhelt, D. (1989) *Proc. Natl. Acad. Sci. U.S.A. 86*, 4943−4947.
Glaeser, R. M., Tong, L., & Kim, S.-H. (1989) *Ultramicroscopy 27*, 307−318.
Han, B.-G., Vonck, J., & Glaeser, R. M. (1994a) *Biophys. J. 67*, 1179−1186.
Han, B.-G., Wolf, S. G., Vonck, J., & Glaeser, R. M. (1994b) *Ultramicroscopy 55*, 1−5.
He, Y., Krebs, M. P., Fischer, W. B., Khorana, H. G., & Rothschild, K. J. (1993) *Biochemistry 32*, 2282−2290.
Henderson, R., Baldwin, J. M., Ceska, T. A., Zemlin, F., Beckmann, E., & Downing, K. H. (1990) *J. Mol. Biol. 213*, 899−929.
Holz, M., Drachev, L. A., Mogi, T., Otto, H., Kaulen, A. D., Heyn, M. P., Skulachev, V. P., & Khorana, H. G. (1989) *Proc. Natl. Acad. Sci. U.S.A. 86*, 2167−2171.
Hoppe, W., & Hegerl, R. (1980) in *Computer processing of electron microscope images* (Hawkes, P. W., Ed.) pp 127−189, Springer, Berlin.
Kataoka, M., Kamikubo, H., Tokunaga, F., Brown, L. S., Yamazaki, Y., Maeda, A., Sheves, M., Needleman, R., & Lanyi, J. K. (1994) *J. Mol. Biol. 243*, 621−638.
Koch, M. H. J., Dencher, N. A., Oesterhelt, D., Plöhn, H.-J., Rapp, G., & Büldt, G. (1991) *EMBO J. 10*, 521−526.
Krebs, M. P., & Khorana, H. G. (1993) *J. Bacteriol. 175*, 1555−1560.
Lanyi, J. K. (1993) *Biochim. Biophys. Acta 1183*, 241−261.
Lozier, R. H., Bogomolni, R. A., & Niederberger, W. (1975) *Biophys. J. 15*, 955−962.
Ludlam, C. F. C., Sonar, S., Lee, C.-P., Coleman, M., Herzfeld, J., RajBhandary, U. L., & Rothschild, K. J. (1995) *Biochemistry 34*, 2−6.
Mathies, R. A., Lin, S. W., Ames, J. B., & Pollard, W. T. (1991) *Annu. Rev. Biophys. Biophys. Chem. 20*, 491−518.
Müller, D. J., Büldt, G., & Engel, A. (1995) *J. Mol. Biol. 249*, 239−243.
Nakasako, M., Kataoka, M., & Tokunaga, F. (1989) *FEBS Lett. 254*, 211−214.
Nakasako, M., Kataoka, M., Amemiya, Y., & Tokunaga, F. (1991) *FEBS Lett. 292*, 73−75.
Needleman, R., Chang, M., Ni, B., Váró, G., Fornés, J., White, S. H., & Lanyi, J. K. (1991) *J. Biol. Chem. 266*, 11478−11484.
Nilsson, A., Rath, P., Olejnik, J., Coleman, M., & Rothschild, K. J. (1995) *J. Biol. Chem. 270*, 29746−29751.
Oesterhelt, D., & Stoeckenius, W. (1974) *Methods Enzymol. 31*, 661−678.
Olejnik, J., Brzezinski, B., & Zundel, G. (1992) *J. Mol. Struct. 271*, 157−173.
Ormos, P., Chu, K., & Mourant, J. (1992) *Biochemistry 31*, 6933−6937.
Otto, H., Marti, T., Holz, M., Mogi, T., Lindau, M., Khorana, H. G., & Heyn, M. P. (1989) *Proc. Natl. Acad. Sci. U.S.A. 86*, 9228−9232.
Otto, H., Marti, T., Holz, M., Mogi, T., Stern, L. J., Engel, F., Khorana, H. G., & Heyn, M. P. (1990) *Proc. Natl. Acad. Sci. U.S.A. 87*, 1018−1022.
Perkins, G. A., Liu, E., Burkard, F., Berry, E. A., & Glaeser, R. M. (1992) *J. Struct. Biol. 109*, 142−151.
Perkins, G. A., Burkard, F., Liu, E., & Glaeser, R. M. (1993) *J. Microsc. 169*, 61−65.
Pfefferlé, J.-M., Maeda, A., Sasaki, J., & Yoshizawa, T. (1991) *Biochemistry 30*, 6548−6556.
Rath, P., Krebs, M. P., He, Y., Khorana, H. G., & Rothschild, K. J. (1993) *Biochemistry 32*, 2272−2281.
Rothschild, K. J., Braiman, M. S., He, Y.-W., Marti, T., & Khorana, H. G. (1990a) *J. Biol. Chem. 265*, 16985−16991.
Rothschild, K. J., He, Y.-W., Mogi, T., Marti, T., Stern, L. J., & Khorana, H. G. (1990b) *Biochemistry 29*, 5954−5960.
Rothschild, K. J., Marti, T., Sonar, S., He, Y.-W., Rath, P., Fischer, W., & Khorana, H. G. (1993) *J. Biol. Chem. 268*, 27046−27052.
Sasaki, J., Shichida, Y., Lanyi, J. K., & Maeda, A. (1992) *J. Biol. Chem. 267*, 20782−20786.
Sonar, S., Krebs, M. P., Khorana, H. G., & Rothschild, K. J. (1993) *Biochemistry 32*, 2263−2271.
Sonar, S., Marti, T., Rath, P., Fischer, W., Coleman, M., Khorana, H. G., & Rothschild, K. J. (1994) *J. Biol. Chem. 269*, 28851−28858.
Soppa, J., Duschl, J., & Oesterhelt, D. (1993) *J. Bacteriol. 175*, 2720−2726.
Steinhoff, H.-J., Mollaaghababa, R., Altenbach, C., Hideg, K., Krebs, M., Khorana, H. G., & Hubbell, W. L. (1994) *Science 299*, 105−107.
Strader, C. D., Fong, T. M., Tota, M. R., Underwood, D., & Dixon, R. A. F. (1994) *Annu. Rev. Biochem. 63*, 101−132.
Subramaniam, S., Gerstein, M., Oesterhelt, D., & Henderson, R. (1993) *EMBO J. 8*, 1−12.
Takei, H., Gat, Y., Rothman, Z., Lewis, A., & Sheves, M. (1994) *J. Biol. Chem. 269*, 7387−7389.
Váró, G., & Lanyi, J. K. (1991a) *Biochemistry 30*, 5008−5015.
Váró, G., & Lanyi, J. K. (1991b) *Biochemistry 30*, 5016−5022.
Váró, G., & Lanyi, J. K. (1991c) *Biophys. J. 59*, 313−322.
Vonck, J., Han, B.-G., Burkard, F., Perkins, G. A., & Glaeser, R. M. (1994) *Biophys. J. 67*, 1173−1178.

BI952663C